ROYAL SOCIETY
OF CHEMISTRY

Check for updates

Infrared emitting and absorbing conjugated polymer nanoparticles as biological imaging probes

Daniel Honeybone,[a] Hannah Peace [iD] [b] and Mark Green [iD] *[c]

The use of conjugated polymer nanoparticles in biological imaging is emerging as an effective method of analysis and diagnosis, with their enhanced optical stability and wide colour pallete a distinct advantage over existing dye systems. Notably, the wide range of materials available include narrow band gap polymers, not originally designed for imaging but with fortuitous electronic properties that can be exploited in clearly defined near-infrared regions, areas of great interest to clinicians and biologists as transparent windows. Traditionally, few materials can be used as convenient probes in the near infrared, however, conjugated polymers provide an immediate solution to imaging in this desirable spectral range.

Introduction

Optical biological imaging is ubiquitous, with a wide range of techniques (and even therapies) based on light emission in the visible spectral region.[1] Almost all branches of biology, diagnostics, therapy, and clinical medicine have applications that use visible luminescence as an optical reporter. Most compounds used in such applications are small organic molecules, which normally exhibit bright emission but are often accompanied with reduced stability and rapid photo-bleaching.[2] Whilst imaging in the visible is routine, near-infrared (IR) investigations have distinct advantages, yet presents more of a challenge.[3–5] This region is important, as tissue, water, and haemoglobins absorb minimally, and background autofluorescence is reduced at these wavelengths, allowing for deep tissue imaging. The three main windows are between *ca.* 700 nm and 950 nm, termed NIR-1: between 1000 nm and 1350 nm, termed NIR-2 and a third, often underused region between 1550 nm and 1870 nm, termed NIR-3 (or NIR-2b). A major stumbling block with imaging in these windows is the availability of brightly emitting, stable small molecule organic fluorophores with indocyanine green (ICG) being the favoured material. Indocyanine green is the only clinically approved IR-emitting dye and has been utilised in imaging since the 1950s yet is relatively unstable and has a quantum yield of 2.5%.[6,7]

The development of new solid-state materials, notably on the nanoscale, has uncovered new luminescent compounds with optical properties in the near-IR that present brighter, more stable options. Notably, semiconductor quantum dots (QDs) have tuneable emission and can access almost the entire visible and near IR spectral regions by a judicious choice of materials, size, and structure.[8] Likewise, carbon nanotubes have been shown to be extremely useful in imaging in the second IR window, with the associated emission even penetrating bone to an overall imaging depth of over 2 mm.[9] Whilst valuable, quantum dots and nanotubes are unlikely to find general acceptance in a clinical environment due to the (possibly ill-perceived) toxicity issues remaining around the use of compounds semiconductors and their metal content, and the fibre-like structure of nanotubes.

Conjugated polymers offer a potential solution.[10] Originally developed for the display applications, they are designed to withstand extensive electrical excitation and are therefore relatively stable and brightly emitting in the visible region. They are however usually insoluble in water, so are typically processed into nanoparticles with an amphiphilic surface species, which allows the introduction of surface functional groups, a desirable feature that facilitates the attachments of antibodies, proteins, peptides, *etc.* for targeted imaging. As conjugated polymers are primarily organic in nature, and (in the case of studies reported in this review) organised into encapsulated nanoparticles, there are no toxicity issues normally associated with, for example, the heavy metal content of inorganic semiconductor quantum dots. There has been, to the best of our knowledge, no specific study into the toxicity of conjugated polymer nanoparticles beyond the engineered particles which are utilised in photodynamic and photothermal

[a] *The Medical School, The Faculty of Medicine, University of Sheffield, Beech Hill Road, Broomhall, Sheffield, S10 2RX, UK*

[b] *Stream Bio Ltd., Alderley Park, Nether Alderley, Cheshire, SK10 4TG, UK*

[c] *Department of Physics, King's College London, The Strand, London, WC2R 2LS, UK. E-mail: mark.a.green@kcl.ac.uk*

Table 1 Polymer/dye nanoparticles described in this review and notes

	Approx. absorption max. wavelength/nm	Approx. emission max. wavelength/nm	Quantum yield/%	Ref
Co-poly(2,3-diphenylthieno[3,4-b]pyrazine-alt-9,9-dioctylfluorene (CDPDOF) + NIR775	600	775	28	13
Poly(9,9-dioctylfluorene-co-benzothiadiazole) (PFBT) + NIR775	450	777	11	15
Poly[2-methoxy-5-(2-ethylhexyloxy)-1,4-phenylenevinylene] (MEH-PPV) + NIR775	500	778	9	16
PF-TC6FQ-BODIPY	495	723	33	17
Poly(fluorene-benzothiadiazole)-BODIPY (PFBT-BODIPY) (Typical example)	708	725	5.9	18
4,7-di(thiophen-2-yl)benzo[c][1,2,5]thiadiazole fused with 1,10-phenanthroline.	575	650	6.2	19
Poly[[9,9-di-n-octylfluor-ene-2,7-diyl]-alt-co-(2,5-bis(4-(N,N-(diphenylmino)styryl) benzene)-1,4-diyl]] (P-F8-DPSB) + DPA-PR-PDI	440	730	45	20
Poly[9,9-bis(6′-(N,N-dimethylamino)hexyl]fluorenyldivinylene-alt-4,7-(2,1,3,-benzothiadiazole)] (PFVBT)	516	636	Not given	21
Poly{[9,9-di(hexyl)fluorene]-alt-co-[4,7-bis(thiophen-2-yl)-2,1,3-benzothiazole]} (PFDBT)	ca. 520	687	13.6	23
Poly[(9,9-dihexylfluorene)-co-2,1,3-benzothiadiazole-co-4,7-di(thiophen-2-yl)-2,1,3-benzothiadiazole] (PFBTDBT10)	ca. 475	698	27	24
Poly(benzo[1,2-b:3,4-b′]difuran-alt-fluorothieno-[3,4-b]thiophene) (pDA)	654	1047	1.7	25
Poly[2,6-(4,4-bis-(2-ethylhexyl)-4H-cyclopenta[2,1-b:3,4-b′]-dithiophene)-alt-4,7-(2,1,3-benzothiadiazole]] (PCPDTBT)	800	900	39	28
	700	865	1.46	39
	703	750	2.8	44
Poly[2-(2,5-dibromo-thiophen-3-yl)-ethyl acetate)-co-4,7-(2,1,3-benzothiadiazole)]	ca. 500	600–730	2.3	29
Poly{[4,4,9,9-tetrakis(4-(octyloxy)phenyl-4,9-dihydro-s-indaceno[1,2-b:5,6-b′]dithiophene]-alt-co-[4,7-di(thiophen-2-yl)-2,1,3-benzothiadiazole} (PIDT-DBT)	600	720	Not given	30
Poly[9,9-di((S)-2-methylbutyl)fluorene)-co-bis(difluoroboron)1,2-bis((1H-pyrrol-2-yl)methylene)hydrazine-co-4,7-di(thiophen-2-yl)-2,1,3-benzothia-diazole (PFBOPHYDBT)	550	675	9	31
PEG-grafted poly(cyclopentadithiophene-alt-diketopyrrolopyrrole) (PCD-PEG)	790	Not relevant	Not relevant	33
PEG-grafted poly(fluorene-alt-diketopyrrolopyrrole) (PFD-PEG)	680	Not relevant	Not relevant	33
TII-TEG	ca. 1350	Not relevant	Not relevant	34
Poly(benzodithiophene-alt-benzobisthiadiazole)	1000	Not relevant	Not relevant	35
Poly(diketopyrrolopyrrole-alt-thiadiazoloquinoxaline)	1200	Not relevant	Not relevant	36
Poly((E)-3-(5-([8,8′-biindeno[2,1-b]thiophenylidene]-2-yl)thiophen-2-yl)-alt-2,5-bis(2-octyldodecyl)-6-(thiophen-2-yl)-pyrrolo[3,4-c]pyrrole-1,4(2H,5H)dione) (PBDP-DPP)	790	650 nm (gold clusters)	5.3	37
PTD	1200	Not relevant	Not relevant	38
Poly[(4,4′-bis(2-ethylhexyl)dithieno[3,2-b:2′,3′-d]silole)-2,6-diyl-alt-(2,1,3-benzothiadiazole)-4,7-diyl] (PSBTBT)	660	980	0.7	39
Poly[[4,8-bis[(2-ethylhexyl)oxy]benzo[1,2-b:4,5-b′]dithiophene-2,6-diyl][3-fluoro-2-[(2-ethylhexyl)carbonyl] thieno[3,4-b]thiophenediyl]] (PTB7)	610	795	0.57	39
Poly[N-9′-heptadecanyl-2,7-carbazole-alt-5,5-(4′,7′-di-2-thienyl-2′,1′,3′-benzothiadiazole)] (PCDTBT)	550	735	7.18	39
Poly[[5-(2-ethylhexyl)-5,6-dihydro-4,6-dioxo-4H-thieno[3,4-c]pyrrole-1,3-diyl][4,8-bis[(2-ethylhexyl)-oxy]benzo[1,2-b:4,5-b′]dithiophene-2,6-diyl]] (PBDTTPD)	543	730	2.68	39
PDFT	800	1000	Not given	43
PBTQ4F and poly[2-methoxy-5(2-ethylhexyloxy)-1,4-(1-cyanovinylene-1,4-phenylene)] CN-PPV blende dual emission particles	900 and 500	1100 and 590	1.9 and 6	45
Fluorinated PBTQ	ca. 925	ca. 950	3.2	46
Pttc-SeBTa-NIR1125/1270/1380	ca. 1100/1200/1300	ca. 1125/1270/1380	0.05–0.18	48

therapy.[11] It should also be noted that significant work has been reported in the field of plastic bioelectronics, where conjugated polymers present flexible, conducting materials that interface favourably with biological tissues.[12] One of the key applications outside of biology for conjugated polymers is plastic electronics and solar energy conversion. As such, specific conjugated polymers have been designed to have narrow band gaps to allow charge carrier injection in solid-state structures, and this serendipitously results in emission towards the near infrared spectral range. Hence, materials originally designed for device applications have found utility in biology, specifically in a niche discipline, where their stable optical properties in a distinct spectral region make them ideal imaging agents. A list of polymer particles and a brief synopsis of their optical properties have been provided in Table 1.

Early work in biological imaging using doped conjugated polymers

The seminal work on conjugated polymer nanoparticles as imaging probes concentrated on materials that emitted in the visible, for obvious reasons. One of the earliest reports exploring the near-IR region described the use of co-poly(2,3-diphenylthieno[3,4-b]pyrazine-alt-9,9-dioctylfluorene (CDPDOF) doped with a dye molecule, (silicon 2,3-naphthalocyanine bis(trihexylsilyloxide), referred to as NIR775).[13] These studies describing the use of conjugated polymers for use in the IR region didn't utilise their inherent optical properties. Rather,

This journal is © The Royal Society of Chemistry 2023

J. Mater. Chem. C, 2023, 11, 7860–7871 | 7861

they used the polymer back bone as a scaffold for energy transfer to an established IR emitter. The particles, synthesised with Tween 20 as a surfactant, displayed an average diameter of 82 nm and a standard deviation of 21 nm and remained stable and unchanged in size in water for over 30 days. The particles emitted at 690 nm with a quantum efficiency of 0.28 without the dye molecule, which shifted to 780 nm through a Förster resonance energy transfer (FRET) process with the inclusion of the dye, the addition of which also more than doubled the emission efficiency (the relatively low quantum yields associated with narrow band gap materials is well known, as explained by energy gap law, where the nonradiative decay rates from triplet states increases with a decreasing energy gap.[14]) An interesting comparison to spectrally analogous inorganic semiconductor quantum dots was made, which highlighted that although the quantum yield of the optimised polymer/dye particles were significantly lower by approximately 20-fold, the extinction coefficient of the conjugated polymer particles was several thousand times larger, ultimately resulting in polymer particles that were two orders of magnitude brighter than QDs. A brief imaging study in mice highlighted no measurable fluorescence signal with just CDPDOF, although emission from dye doped particles were clearly observed, with the particles accumulating in the liver after 120 minutes. It is worth highlighting a similar report, also in 2011, that described a similar material, but with no specific biological imaging described.[15] In this case, the same dye molecule was doped into the commercially available conjugated polymer poly(9,9-dioctyl-fluorene-co-benzothiadiazole) PFBT, a standard yellow emitter, which exhibited excellent energy transfer to the dye despite inefficient spectral overlap. The resultant particles, capped with polystyrene/polyethylene glycol (PEG) carboxylate, emitted at 777 nm with a quantum yield of ca. 0.11 and a slight contribution from the polymer host, in a similar manner as the report by Aoki. The particles were comparable in size (ca. 18 nm) to commercially available quantum dots that emitted at 800 nm yet were four times brighter. To test stability, the particles were incubated in human blood plasma and (4-(2-hydroxyethyl)-1-piperazineethanesulfonic acid) (HEPES) buffer at 37 °C for 72 hours, with no leakage of the dye molecule observed. It was noted that the conjugated polymer-based particles had exceptionally large two-photon absorption cross sections, which together with the large Stokes shift made the particles ideally suited for two-photon imaging.

The idea of using the naphthalocyanine dopant with a common conjugated polymer was extended to the use of poly[2-methoxy-5-(2-ethylhexyloxy)-1,4-phenylenevinylene] (MEH-PPV), a common red emitter, as a host in the preparation of 30–40 nm particles.[16] In this example, MEH-PPV was doped with NIR775 using polystyrene/PEG carboxylate as the surface species, pushing the emission again out to ca. 780 nm with a quantum yield of ca. 0.09. To the surface was conjugated Luc8, a bioluminescent enzyme which was used to excite the core conjugated polymer when exposed to enzyme's substrate (coelenterazine) through a bioluminescence resonance energy transfer (BRET) process. The excited conjugated polymer in turn excited the dye which emitted in the near IR region as expected. Also added to the surface was an arginylglycylaspartic acid (RGD) peptide to target human glioblastoma U87MG. Intravenous tail vein injection of the particles and substrate into nude mice with a xenografted U87MG tumour resulted in in situ-excited strong bioluminescence in the very small subcutaneously implanted tumours (2 or 3 mm in diameter) and clear imaging after 5 minutes, with a tumour-to-background ratio of over 100. It was also noted that the particles without the Luc8 could be used to map the lymphatic system using standard imaging techniques; 48 h after injection of the particles, fluorescent imaging revealed uptake in lymph nodes, skin, stomach, bone, liver, spleen and tumour. The NIR fluorescence signal was also observed in collected urine, suggesting that the particles cleared through renal system as well as the hepatobiliary system. The use of phthalocyanine dyes has been extended to the inclusion of such compounds and related – BODIPY – on a polymer backbone. In elegant work by Ke et al., a polymer was designed with a donor–bridge–acceptor system (fluorene-π bridge-phthalocyanine/BODIPY) which also included carboxylic acid on the polymer backbone, negating the need for an additional surfactant.[17] This polymer was simply injected in water under sonication, forcing a nanoprecipitation event resulting in 26 nm particles (±3 nm). The pendant carboxylic acids groups could then be linked to streptavidin and then antibodies via carbodiimide coupling and biotinylation. The particles emitted primarily at ca. 720 nm, with quantum yields up to 33%, depending on the structure. The emission, which was as narrow as 29 nm full width at the half the maximum (FWHM), was compared to similar commercially available quantum dots, and found to be up to three time brighter. The resulting particles were used to image zebrafish, and mouse tumours via folic acid/folate receptors for up to 36 days, maintaining 32% of their emission intensity. Similar work reported the use of a BODIPY, fluorene and benzothiadiazole random copolymer in the preparation of nanoparticles. In this example, side chains of PEG and PEG terminated with folic acid were added to the polymer backbone, again negating the need for a further surfactant. A tetrahydrofuran (THF) solution of the polymer was then slowly added to water followed by sonication, resulting in nanoparticle formation. The emission was tuneable by controlling the structure of the polymer, with emission between ca. 725 nm to ca. 825 nm which was used in imaging folate-receptor positive cancer cells.[18] An interesting similar development by Yan et al. was the development of a donor/acceptor (D–A) copolymer based on thiophene fused 1,10-phenanthroline.[19] In this system, the phenanthroline subunit was excited, and energy transfer occurred through the fluorene unit, with emission at ca. 650 nm. When processed into notably small polystyrene(maleic anhydride) (PSMA) functionalised polymer nanoparticles (P-dots) of only 13 nm (as determined by dynamic light scattering), the particles emitted at ca. 677 nm, with an absolute quantum yield of 6.2%, higher than commercially available dyes. The surface of the particles was further functionalised with streptavidin and then incubated with HeLa cells (after the cells had been incubated with biotinylated monoclonal anti-alpha tubulin

7862 | J. Mater. Chem. C, 2023, 11, 7860–7871

This journal is © The Royal Society of Chemistry 2023

antibodies) and specific targeting onto subcellular structure was confirmed by wide field microscopy.

More recent examples of dopants being used in conjugated polymers include a report by Lv *et al.* in 2015, where the conjugated polymer poly[[(9,9-di-*n*-octylfluor-ene-2,7-diyl)-*alt*-co-(2,5-bis(4-(*N*,*N*-(diphenylmino)styryl) benzene)-1,4-diyl)] (P-F8-DPSB) was used with the organic IR-emitting dye DPA-PR-PDI.[20] This pairing might be considered unusual as there is a lack of spectral overlap between the emission of the polymer and the absorption of the dye – essential for the transfer mechanism, ultimately resulting in emission from the dopant molecule. The polymer, which absorbed in the blue spectral region could undergo two-photon absorption, meaning the material could be excited by a near-IR excitation source, bypassing biological background absorption phenomena which hinders some excitation and emission processes. The resulting doped nanoparticles nevertheless had excellent transfer efficiency, with emission at *ca.* 730 nm and quantum yields of up to 45%. The particles were passivated with Pluronic F127 and linked to folate groups to target folic acid receptors in HeLa cells. Upon excitation, the particles were found to be extremely photostable under 30 minutes of continuous laser illumination and could penetrate an impressive 1200 μm. Toxicity studies highlighted less than 5% decrease in cell viability when the HeLa cells were treated with nanoparticles of 10 μg mL^{-1} concentration.

Following these initial developments where additional organic compounds were included in the particles, poly[9,9-bis-(6'-(*N*,*N*-dimethylamino)hexyl)fluorenyldivinylene-*alt*-4,7-(2,1,3,-benzothiadiazole)] (PFVBT) in combination with iron oxide, encapsulated in a mixture of poly(lactic-*co*-glycolic-acid)-poly(ethylene glycol)-folate (PLGA-PEG-FOL) and poly(lactic-*co*-glycolic acid) (PLGA) was used in near IR imaging using the polymer alone as the light emitting agent.[21] The nanoparticles, *ca.* 180 nm diameter exhibited superparamagnetic properties and reportedly bright fluorescence with absorption and emission maxima at 516 and 636 nm. The particles also exhibited superparamagnetic behaviour at 298 K with a saturated magnetization value of 3.42 emu g^{-1}, which was sufficient for *in vivo* magnetic resonance imaging. It was suggested that the iron oxide particles were separated from the conjugated polymer to minimize fluorescence quenching. The targeting ability of nanoparticles was studied by using MCF-7 breast cancer cells, with the folic acid on the surface of the particles resulting in the particles being internalized into the cell cytoplasm, with more than 99% of the cells effectively stained by the materials. It was also reported that there was approximately 100% cell viability with extremely low cytotoxicity after 48 and 72 hours. The particles were also administered to H22 tumour bearing mice *via* injection in the tail vein, where particle accumulation in hepatoma reached a maximum at 6 h post injection. The particles were found to preferentially accumulate in tumour tissues through the enhanced permeability and retention (EPR) effect *via* folate receptor-mediated active targeting effect. (It should be noted that the validity of EPR effect model is currently a matter of some debate, with recent reports highlighting that endothelial transcytosis maybe the dominant mechanism rather than the suggested passive process[22]). Iron content in the tumour verified the effectiveness of the folate targeted uptake, with magnetic resonance images of the tumour confirming the optical studies. It is also worth highlighting that most of the particles could be excreted from the body after imaging, suggesting positive biocompatibility.

This was followed by reports by Liu, who described the use of poly{[9,9-di(hexyl)fluorene]-*alt*-*co*-[4,7-bis(thiophen-2-yl)-2,1,3-benzothiazole]}, PFDBT, as a near IR emitting conjugated polymer (emission maxima = 687 nm), which was processed into polymer particles using the phospholipid 1,2-distearoyl-*sn*-glycero*-3-phosphoethanolamine-*N*-[amino(polyethylene glycol)$_{2000}$ (DSPE-PEG$_{2000}$) and DSPE-PEG$_{2000}$-maleimide capping agents.[23] A significant observation was the reduction in emission quenching when polyhedral oligomeric silsesquioxane (POSS) was added to the polymer and the resulting polymer processed into nanoparticles. The POSS-terminated polymer particles exhibited quantum yields of *ca.* 13.6%, as opposed to *ca.* 2% for those without the bulky group. Conjugation of the maleimide functionality with anti-HER2 affibodies allowed the particles to selectively target SKBR-3 cancer cells. Under constant illumination, the polymer particles were found to be significantly more stable that Rhodamine 6G, and comparable to quantum dots. Importantly, even at high concentrations (20 nM), cytotoxicity was shown to be negligible. The same group also reported the use of a similar conjugated polymer, poly[[(9,9-dihexylfluorene)-*co*-2,1,3-benzothiadiazole-*co*-4,7-di(thiophen-2-yl)-2,1,3-benzo-thiadiazole] (PFBTDBT10), with essentially the same backbone, but with differing side groups.[24] The material was again encapsulated in DSPE-PEG, but this time, with a pendant folate group. The particles, 80 nm in (hydrodynamic) diameter had an emission maximum at 698 nm and an unusually large Stokes shift of 233 nm, allowing excellent separation of excitation and emission. The particles had a quantum yield of 0.27, larger than comparable quantum dots. The evaluation of the particles including blood circulation half-life, non-invasive targeted *in vivo* fluorescence imaging and cancer diagnosis, major tissue/organ imaging as well as *in vivo* toxicities revealed that the particles were safe and efficient fluorescent probes for *in vivo* applications. Specifically, the particles clearly targeted MCF-7 breast cancer cells, and in tumour tissue in H22 tumour bearing ICR mice, attributed to passive targeting. Cytotoxicity experiments in the mice highlighted the particles were safe, even with particle accumulation in the liver and spleen. With regards to the optical properties, the particles exhibited strong photobleaching resistance, with only a 2% decrease in photoluminescence intensity after 10 mins of 543 nm laser excitation, similar to Qdot 655 and better than Alexa Fluor 555 and Rhodamine 6G. With regards to thermal stability, the particles were incubated at 37 °C for 7 days in phosphate buffer solution, and showed no decrease in emission, unlike Qdot 655, Alex Fluor 555 and Rhodamine 6G, all of which decreased by between 18% and 49%. There was also no observable change in diameters, highlighting the biostability.

Emission from low band gap polymers

As described above, many early materials might not be strictly considered as true IR-emitting conjugated polymer nanoparticles, as in some cases, the emitting species was a dopant. A key report by Hong et al. highlighted the use of a low band gap donor/acceptor co-polymer with emission at 1050 nm, poly(benzo[1,2-b:3,4-b′]difuran-alt-fluorothieno-[3,4-b]thiophene), (pDA) in nanoparticle formation, along with DSPE-PEG as a capping agent.[25] The conjugated polymer used is notable for being one of the first materials specifically engineered via the donor/acceptor strategy towards low band gap conjugated polymers[26] for use in biological imaging rather than for use in solid state applications, where low band gap polymers are highly desirable.[27] (It should be noted that the majority of low band gap polymer materials used in biological imaging and addressed in this report are structured in this manner.) The resulting particles were extremely small, measured at 2.9 nm diameter using atomic force microscopy and could be tuned to have hydrodynamic diameters of less than 6 nm. The particles exhibited an absorption maximum at 654 nm and an emission maximum at ca. 1050 nm, a significant Stokes shift of 400 nm. The emission quantum yield surprisingly remained unaltered when the polymer was processed into particulate form (ca. 1.7%), which was stable with over 1 hour continuous excitation. Attachment of thiolated Cetuximab (Erbitux) antibodies to particles functionalised with DSPE-PEG-NH$_2$ resulted in nanoparticles that exhibited targeting capability towards the epidermal growth factor receptors (EGFRs) on EGFR-positive breast cancer tumour cells MDA-MB-468. It was also noteworthy that the particles could be used to track blood flow in capillaries of less than 10 mm diameter, which is less than the resolution available via ultrasound and optical coherence tomography. Consistent with other studies of toxic or health effects in animals injected with conjugated polymer nanoparticles, no adverse effects were observed over a 2-month period.

This polymer was not, however, commercially available. The earliest report of IR emission in the first biological window using a readily available conjugated polymer utilised poly[2,6-(4,4-bis-(2-ethylhexyl)-4H-cyclopenta[2,1-b:3,4-b′]-dithiophene)-alt-4,7-(2,1,3-benzothiadiazole]] (PCPDTBT).[28] In this example, the polymer and a phospholipid were mixed together in chloroform and left to evaporate under nitrogen in a sample vial. The dry material was then transformed into nanoparticles by sonication of the vial in water. The resulting nanoparticles were approximately 60 nm ± 20 in diameter in water, with an absorption maximum at ca. 800 nm, and an emission maximum at ca. 900 nm (quantum yield of 0.39), both of which are significantly shifted to the red spectral region relative to the chloroform solution. The particles were then used to image HeLa cells, but notably were also used in phototherapy. It was observed that heat was generated by the nanoparticles upon photoexcitation, with dead cells imaged at particle concentrations of 0.1 mg mL^{-1} and a lasing power of 8 W cm^{-2} making the particles theranostic in nature.

An early example of pH responsive conjugated polymer nanoparticles was reported by Pennakalathil et al., where poly[2-(2,5-dibromo-thiophen-3-yl)-ethyl acetate)-co-4,7-(2,1,3-benzothiadiazole)], a conjugated polymer with carboxylic acid side groups was transformed into nanoparticles by injection of a THF solution into water, without the need for an additional capping agent.[29] The particles, 56 nm in diameter, had an emission maxima at 717 nm and a quantum yield of 2.3, yet the optical properties were not the main goal of this paper. By including the water-insoluble anti-cancer drug camptothecin in the phase transfer step, the drug was internalised into the structure of the particle. The size of the particles was increased to 180 nm by altering the pH to 5.0. A study into drug release from the particles with different loadings highlighted pH 5, comparable to the mild acidity observed in tumour micro-environments, as the fastest method of release as opposed to pH 7.4. Whilst light emission was observed from particles internalised in hepatocellular carcinoma Huh7 cells, this was not reported in any depth.

In 2015, Liu et al. reported the synthesis of poly{[4,4,9,9-tetrakis(4-(octyloxy)phenyl-4,9-dihydro-s-indaceno[1,2-b:5,6-b′]di-thiophene]-alt-co-[4,7-di(thiophen-2-yl)-2,1,3-benzothiadiazole]} (PIDT-DBT), which could be transformed in nanoparticles with a hydrodynamic diameter of 56 nm, which remained unchanged for over 14 days in buffer solution.[30] The particles exhibited an absorption maximum at 600 nm with an emission maximum at 720 nm in water, and displayed a significant Stokes shift of 120 nm, which allowed the minimisation of background interference. The long absorption tail, extending to over 750 nm, allowed excitation in the near-IR. Addition of cell penetrating peptides to the particle surface allowed the particles to trace HepG2 liver cancer cells over 8 days and monitor liver tumour growth for over 27 days. Of note was the imaging depth; 230 μm, when excited at 590 nm. When compared to commercially available quantum dots (Qtracker 705), the conjugated polymer particles showed a longer tracking period and brighter emission intensity. The presence of the peptide was essential for the targeted imaging of the internalisation into the cytoplasm of the cells. Further evidence of the targeting ability was the lack of emission detected from the liver tissue of mice with no HepG2 cells. The cytotoxicity was explored using an MTT assay and found to be negligible.

A further interesting development was the synthesis and use of poly[9,9-di((S)-2-methylbutyl)fluorene)-co-bis(difluoroboron)-1,2-bis((1H-pyrrol-2-yl)methylene)hydrazine-co-4,7-di(thiophen-2-yl)-2,1,3-benzothia-diazole (PFBOPHYDBT), a chiral conjugated polymer in nanoparticle synthesis.[31] The polymer had an absorption maximum at ca. 525 nm, which red shifted upon nanoparticle formation to ca. 550 nm. The emission of the free polymer was ca. 625 nm, which shifted to ca. 675 nm again on nanoparticle formation. The particles were formed by injection of THF solutions into water without an additional capping agent, yielding particles, the size of which (between ca. 80 and 200 nm) could be varied by altering the polymer concentration in the starting solution. Particles with diameters of ca. 80 nm (with a quantum yield of 9%) were used in imaging HeLa cells, accumulating at the edge of the cytoplasm and were able to withstand 10 minutes of constant laser illumination,

exhibiting only a 7% drop-off in intensity. The particles also showed a low cytotoxicity. Interestingly, the particles also displayed a size dependant chirality, although further details regarding the use of chiral particles were not provided.

Photoacoustic imaging

Another imaging modality worth mentioning is photoacoustic (PA) imaging, where ultrasound waves are detected after being generated by laser pulses, where again, the biological spectral window is an advantage. Photoacoustic imaging is also known to have superior penetration and resolution compared to standard optical imaging, with PA penetration depth often measured in centimetres, and PA imaging resolution routinely measured in micrometres. Conjugated polymer particles with optical properties in the IR region have been shown to be excellent contrast agents for PA imaging in deep tissue, and this has been discussed elsewhere.[32] Cui *et al.* reported the synthesis of amphiphilic conjugated polymers PEG-grafted poly(cyclopentadithiophene-*alt*-diketopyrrolopyrrole) (PCD-PEG) and PEG-grafted poly(fluorene-*alt*-diketopyrrolopyrrole) (PFD-PEG), notable for having the PEGylated side chain grafted onto the polymer backbone rather than incorporated into the particle as a separate entity.[33] This elegant approach allowed the polymers to be dispersed in phosphate buffer solution whereupon they self-assembled into nanoparticles, *ca.* 30 to 40 nm in diameter. Particles of PCD-PEG had absorption maxima at *ca.* 790 nm, whilst PFD-PEG exhibited a maximum at *ca.* 680 nm. Laser induced heating of PCD-PEG showed a significant photothermal effect when excited at 808 nm, with a maximum temperature of 86 °C and photothermal conversion efficiency of 37%. As PCD-PEG displayed the superior photothermal properties, it was explored for PA imaging of tumours in live mice, with the PCD-PEG particles clearly visible in tumours after 2 hours of intravenous administration. After 24 hours post administration, the PA signal was found to be seven times the background signal. A similar approach was taken by Wu *et al.*,[34] who similarly prepared a novel thienoisoindigo (TII)-based conjugated polymer (with triethylene glycol (TEG) side chains) which exhibited strong absorption between *ca.* 1000 nm and 1350 nm and a strong PA signal over the entire NIR-II region. Despite the presence of the TEG side chain, DSPE-PEG2000 was used as a capping agent when the particles, *ca.* 86 nm in diameter, were prepared by a nanoprecipitation method. Imaging was confirmed in the dorsal area of rats. Further confirmation was achieved by injecting the particles directly into PC3-M xenografts in mice, where the presence of the particles resulted in an enhancement of the PA signal by *ca.* 7-fold at 1100 nm and *ca.* 13.3-fold at 1300 nm (PA signals from blood vessels surrounding the tumour were observed at 800 nm and 1000 nm). It was further noted that when compared to copper sulfide nanoparticles, 2.5 times less mass concentration of the polymer particles were required to image to the same depth of 5 cm at 1064 nm, with only half the laser energy density.

Other polymers, based on donor/acceptor structures have also been reported for use in photoacoustic imaging.[35] A report by Guo *et al.* highlighted that a polymer, poly(benzodithiophene-*alt*-benzobisthiadiazole), based on benzodithiophene monomers had an absorption band at *ca.* 1000 nm, and, when transformed into nanoparticles (50–60 nm in diameter) capped with a lipid, was an effective photoacoustic imaging agent. Impressively, the material was used to image orthoptic brain tumours through a mouse skull using a 1064 nm excitation source. The particles showed a strong PA signal when internalised by U87 glioma cells, at concentrations as low as 1000 cells. Brain tumours in mouse models were visible after 2 hours post injection in the subcutaneous tissue, with the tumour at a depth of 3.4 mm below the skull. After 24 hours post injection, the tumour could be clearly imaged with a 94-fold increase in the PA signal, more than twice that of MoS_2 based brain imaging agents. These results clearly indicated the uptake of the particles in the tumour and the ability to cross the blood brain barrier. No toxicity was observed.

Photoacoustic imaging in the second biological window was also achieved using poly(diketopyrrolopyrrole-*alt*-thiadiazoloquinoxaline), a donor/acceptor polymer with an absorption maxima at *ca.* 1200 nm, which was processed into particles, *ca.* 50 nm in diameter using an amphiphilic copolymer based on PEG. These particles were also used to image a rat brain, although not through the skull. The signal to noise ratio was found to be 1.5 times higher in the second IR window when imaging brain tissue at depths of up to 3 cm, than when using the same polymer without the quinoxaline group in the polymer back bone (resulting in a material an absorption maximum at *ca.* 750 nm.)[36] In a further study, a similar polymer, poly((*E*)-3-(5-([8,8'-biindeno[2,1-*b*]thiophenylidene]-2-yl)thiophen-2-yl)-*alt*-2,5-bis(2-octyldodecyl)-6-(thiophen-2-yl)-pyrrolo[3,4-*c*]pyrrole-1,4(2*H*,5*H*)dione) (PBDP-DPP) was used but with a protein capping layer on the surface of the resulting nanoparticles rather than the usual surfactants, giving a large number of available functional groups with a notably small hydrodynamic diameter of under 12 nm.[37] The protein modified particles had an absorption maximum at *ca.* 790 nm. To make the particles multimodal, fluorescent gold particles were grown on the surface protein, giving particles that were both luminescent and photo-acoustically active. Tail vein injections of the particles into 4T1 tumour-bearing nude mice resulted in the uptake of the particles (as confirmed by both photoacoustic and fluorescent imaging) not only in the tumour, but also the kidney and liver with a particularly strong signal observed in the kidneys, suggesting renal clearance. In a related study, a polymer from the same family was used to prepare DSPE-PEG capped nanoparticles *via* microfluidic synthesis rather than the standard bench top nano-precipitation, yielding nanoparticles that were tuneable between 42 nm and 132 nm in diameter.[38] The resulting particles were then used in a detailed photoacoustic study, highlighting in high contrast 3-D, the cerebral and tumour vasculatures in nude mice, notably allowing the detection of tumour angiogenesis (Fig. 1). Again, using the second optical window, deep brain tissue could be imaged through the skull.

This journal is © The Royal Society of Chemistry 2023

J. Mater. Chem. C, 2023, **11**, 7860–7871 | **7865**
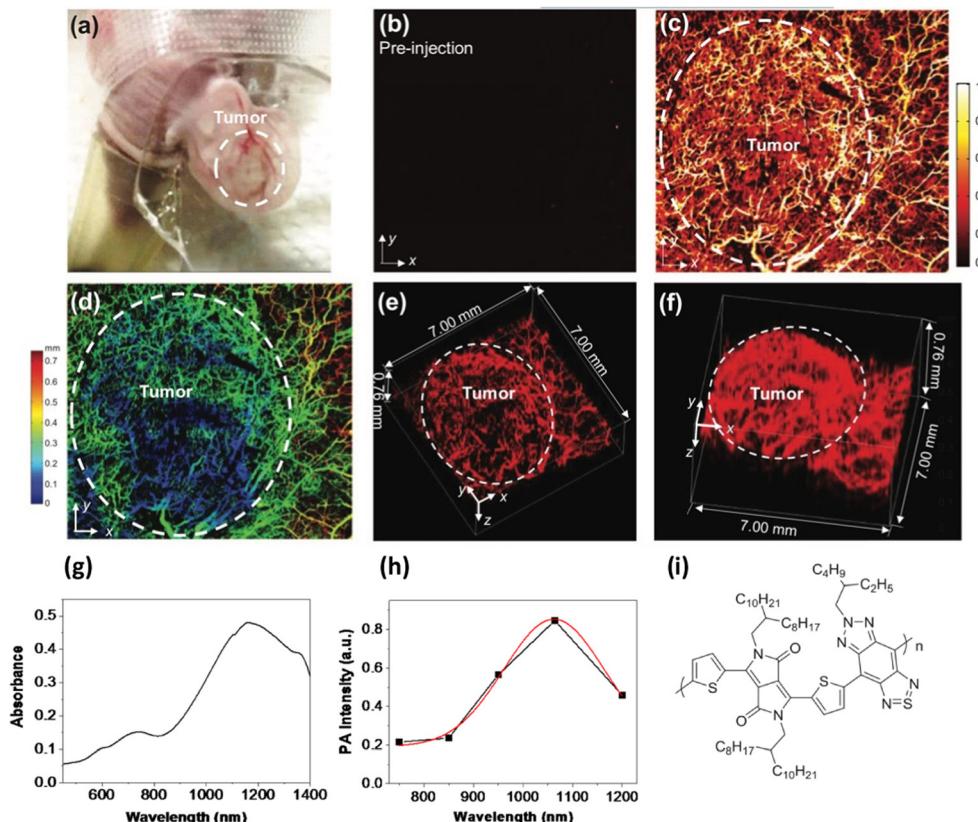
Fig. 1 (A) Photo of a mouse ear with a HepG2 tumour. (B and C) Photoacoustic images of the tumour before and after particle injection. (D) Depth-encoded amplitude projection of image C. (E and F) Three-dimensional reconstruction of ear vasculature, with tumour margin highlighted in a white dashed circle. (G) Absorption spectrum of polymer. (H) Photoacoustic spectrum of polymer. (I) Polymer Structure.[38] Images used with permission from John Wiley and Sons.

Particles prepared using readily available low band gap polymers – and engineered structures

In a notable paper in 2018, a range of standard commercially available low band gap polymers, usually used in photovoltaics, were processed into nanoparticles in water.[39] This paper is significant as unlike most reports mentioned above, these polymers were well known, readily available and used in disciplines other than biology. The common polymers, poly[2,6-(4,4-bis(2-ethylhexyl)-4H-cyclopenta [2,1-b:3,4-b′]dithiophene)-alt-4,7(2,1,3-benzothiadiazole)] (PCPDTBT), poly[[(4,4′-bis(2-ethyl-hexyl)dithieno[3,2-b:2′,3′-d]silole)-2,6-diyl-alt-(2,1,3-benzothiadi-azole)-4,7-diyl] (PSBTBT), poly[[4,8-bis[(2-ethylhexyl)oxy]benzo-[1,2-b:4,5-b′]dithiophene-2,6-diyl][3-fluoro-2-[(2-ethylhexyl)carb-onyl] thieno[3,4-b]thiophenediyl]] (PTB7), poly[N-9′-heptade-canyl-2,7-carbazole-alt-5,5-(4′,7′-di-2-thienyl-2′,1′,3′-benzothia-diazole)] (PCDTBT) and poly[[5-(2-ethylhexyl)-5,6-dihydro-4,6-dioxo-4H-thieno[3,4-c]pyrrole-1,3-diyl][4,8-bis[(2-ethylhexyl)-oxy]-benzo[1,2-b:4,5-b′]dithiophene-2,6-diyl]] (PBDTTPD), were phase transferred (separately) into water without the use of a surfactant, resulting in particles approximately 100 nm in diameter. All the resulting nanoparticles had emission beyond 700 nm, red-shifted from their parent polymers in organic solution, whilst PSBTBT particles notably emitted at 980 nm. Emission quantum yields were reduced in the particulates, although

PCDTBT had a reported quantum yield of 7.18%, notably high when compared to existing IR dyes. The particles were used to label macrophage cells, where the particles were found to be efficiently internalised, although not into the nucleus.

As particle structures become more advanced, and the processability of particles and their associated morphologies become more engineered, applications beyond imaging start to be realised. A report by Li *et al.* highlighted the use of conjugated polymers, in this case termed a semiconducting polymer brush.[40] In this example, alkyl side chains, polyethylene glycol chains, and fluorinated polyethylenimine were grafted to the initial conjugated polymer backbone. This amphiphilic polymer was then injected into water, along with dexamethasone (which targets nuclear glucocorticoid receptors) and CRISPR/Cas 9 cassettes (which interacted with the polyethylenimine through electrostatic interaction) which were then self-assembled into the nanoparticles, approximately 120 nm in diameter. The resulting particles had an absorption maximum at *ca.* 750 nm and emission between 1000 nm and 1400 nm, with a maximum at 1100 nm and a quantum yield of 0.23%. The polymer backbone acted as a photothermal transducer, whereupon laser exposure, the particles fragmented, releasing *ca.* 75% of the cargo within two hours (as opposed to 30% without laser exposure). Lentivirus engineered green

7866 | *J. Mater. Chem. C*, 2023, **11**, 7860–7871

This journal is © The Royal Society of Chemistry 2023

fluorescent protein (GFP)-expressing HCT-116 cells in xeno-grafted tumour bearing mice were used as a model system, with the gene editing capability measured by the reduction in GFP emission. Approximately 30% of cells exhibited reduced GFP emission upon exposure to the editing agent. It was highlighted that incorporating the CRISPR/Cas9 cassettes particles into a nanoparticle reduced the instability usually observed due to DNase and RNase degradation. The cells also showed bright near-IR emission after 15 minutes post intratumoral administration, and further signals were observed in the liver and spleen. This paper notably highlights that even the latest genetic technologies can be combined with semiconducting polymer technology.

One overlooked, yet key issue that dictates the successful use of any nanoparticle in biology is the surface – and surface interface. The majority of the aforementioned papers utilise a capping agent, usually an amphiphilic polymer that interdigitates with the underlying emitting polymer whilst presenting an external functional group on the surface, providing both a conjugation point and stability in aqueous solution. This can be seen as an extension of previous work on inorganic quantum dots, where hydrophobic particles were wrapped in similar compounds, inducing phase transfer.[41] However, this kind of phase transfer for nanoparticles wasn't the first accepted method. Encapsulation in silica, as pioneered by Mulvaney,[42] was also an early route, however, it was relatively difficult from a synthesis perspective compared to overcoating particles with an amphiphilic polymer. One particular issue with conjugated polymer particles is their lack of uniformity. Polydispersed samples are undesirable, as obtaining a population of particles with a known and consistent valency is difficult. Lu et al. have developed a general synthesis of conjugated polymer nanoparticles encapsulated in mesoporous silica with a PEGylated surface and a well-defined particle size and shape.[43] This was achieved by initially phase transferring the hydrophobic polymers to water using a simple surfactant, cetyltrimethyl ammonium bromide (CTAB), forming nanoparticles. Onto these seeds, tetraethyl orthosilicate was hydrolysed, followed by the condensation of further silica, the pores of which were directed by the CTAB, resulting in mesoporous particles. The addition of silane-PEG resulting in the attachment of the ligand to the particle surface. The resulting particles showed evidence of pore formation and were in the range 30–50 nm. The polymer PCPDTBT and a diketopyrrolopyrrole based polymer, PDFT, were encapsulated as described and found to have emission spectra at 820 nm and 1050 nm respectively. Although values weren't provided, it was reported that quantum yields were higher than when encapsulated in DSPE-PEG, a commonly
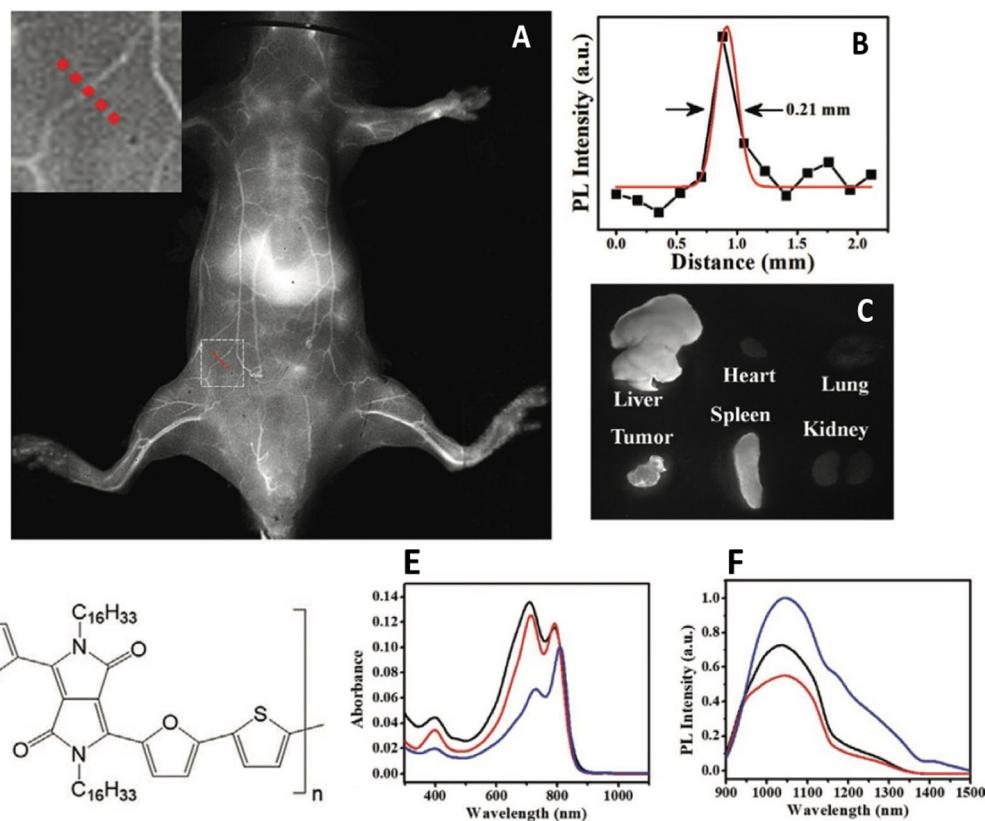
Fig. 2 (A) In vivo near-IR2 image of depilated BALB/c mouse five minutes after the administration of mesoporous silica nanoparticles containing an IR-emitting conjugated polymer. Inset – Cross sectional line. (B) Cross section emission intensity across dotted line in A). (C) Emission from harvested organs 24 hours after intravenous injection. (D) Polymer structure. (E) Absorption spectra of polymer. (F) Emission spectra of polymer.[43] Images used with permission from John Wiley and Sons.

This journal is © The Royal Society of Chemistry 2023

J. Mater. Chem. C, 2023, 11, 7860–7871 | 7867

used lipid. Silica encapsulated PDFT nanoparticles were then used to image 4T1 tumours in BALB/c mice, and were found in the tumour, liver, and spleen (Fig. 2). The pores of the mesoporous silica were also used to adsorb and deliver an anticancer drug, DOX, which was released when the particles were in differing pH environments.

The reduction in emission quantum yield, due to chain folding and intra chain interactions when the light emitting polymer is processed into particulate form, as described above, is another potential problem. Despite this, the particles are usually strongly emissive, although their full potential is clearly not always realised. The search for a system where the conjugated polymer chain packing and orientation into folded structures is reduced is a key direction of research. Elegant work by Modicano *et al.* explored the incorporation of near-IR emitting conjugated polymers (poly(2,5-di(hexyloxy)cyanoterephthalylidene), CN-PPV, and PCPDTBT) into the liquid mid-chain triglyceride core of lipid nanoparticles, the synthesis of which resulted in particles with a diameter of *ca.* 32 nm, that were stable for over 21 days.[44] The dispersion of the polymers in a liquid core rather than the typical solid packed core resulted in a lack of emission quenching, a significant result that will undoubtedly be adopted in future studies.

Most *in vivo* oncology studies report the uptake of CPNs in tumours, and often, additionally, the liver and spleen which is common in nanoparticulate systems. A recent study has highlighted however that small particles (*ca.* 15 nm) composed of a blend of orange emitting and IR emitting polymers and capped with poly(styrene-*co*-maleic anhydride), (PSMA), were accumulated in bone following tail vein injection into a mouse.[45,46] The same PEGylated particles showed general imaging of the vascular system and gradual uptake in the liver and spleen. Likewise larger particles of 25 nm diameter showed less bone accumulation, whilst 50 nm and 100 nm particles showed no bone accumulation at all (Fig. 3). Further studies uncovered that the small particles did not actually bind to bone mineral but were taken up by the endothelial cells in sinusoidal bone marrow and remained for at least 35 days. One interesting detail of the particles was the observation of dual emission – the particles exhibiting both orange/red emission at *ca.* 600 nm, (quantum yield *ca.* 6%) whilst the IR component emitted at *ca.* 1000 nm (quantum yield *ca.* 1.9%). Previous reports of blended conjugated polymer particles showed only one predominant emissive species or shifted emission due to multistep energy transfer.[47] In this case, both species were observed. Whilst this is undoubtedly due to a band energy alignment effect, it does however highlight that the photophysics behind conjugated polymer particles can be engineered to exploit differing imaging modalities.

In 2021, Liu *et al.* reported a significant advance in designing a new conjugated polymer system with bulky side groups to
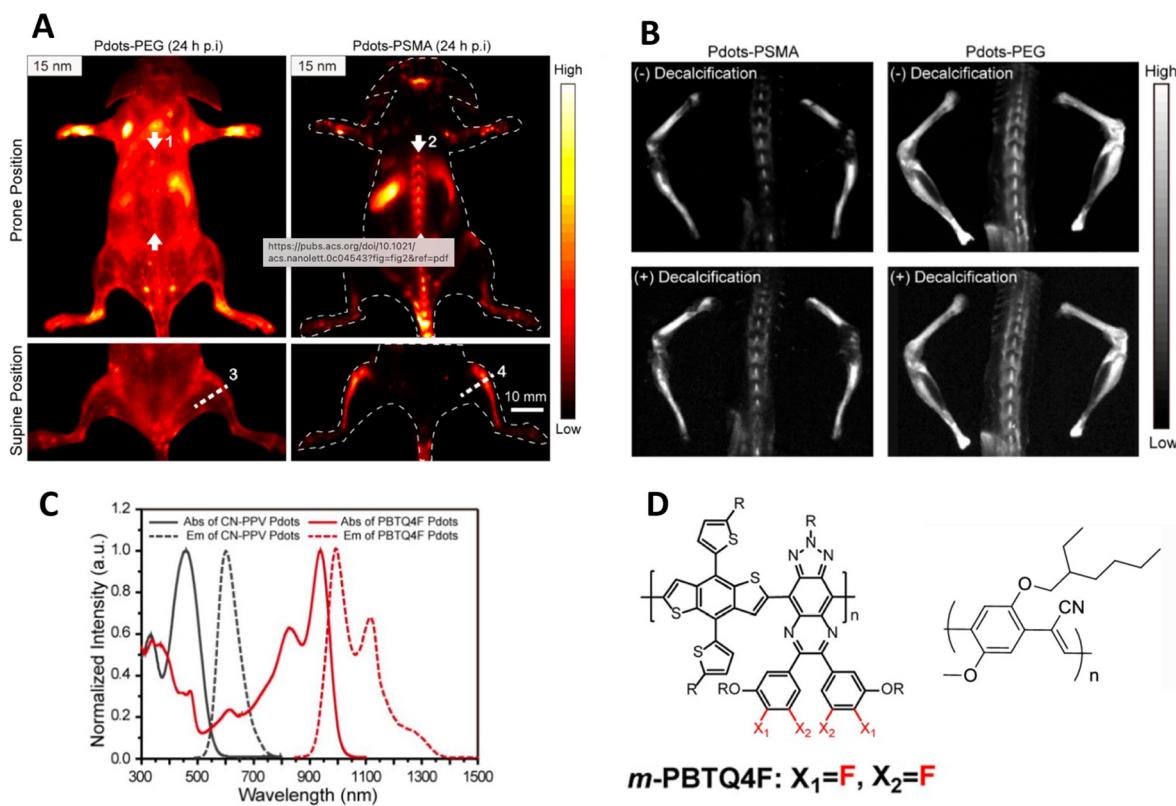
Fig. 3 (A) *In vivo* near-IR2 image of mouse injected with particles capped with either PEG or PSMA. (B) Near-IR2 images of femur, tibia and spine after injection of particularly small particles (*ca.* 15 nm diameter), highlighting bone uptake of particles. (C) Optical properties of polymers used in this study. (D) Structures of polymers used in this study.[45,46] Adapted with permission from *Nano Letters*, 21(1), pp. 798–805. Copyright 2020 American Chemical Society and John Wiley and Sons.

7868 | *J. Mater. Chem. C*, 2023, **11**, 7860–7871

This journal is © The Royal Society of Chemistry 2023

prevent aggregation induced quenching.[48] These novel structures were composed of an anti-aggregation unit - a π-bridge (SeBTa), a polymethine fluorene unit (which was functionalised with carboxylate groups, which were then linked to IR emitting dyes and provided the emissive species rather than the polymer itself), which also acted as an IR-light harvesting unit. The resulting structures exhibited both absorption (between *ca.* 1000 nm and 1350 nm) and emission (between *ca.* 1100 nm and 1450 nm) in the NIR-2 region, with quantum yields between 0.25 and 1.2%. Whilst the measured quantum yield might be considered rather low, the brightness was found to be 1–2 orders of magnitude higher than some typical organic dye molecules. One benefit of these structures was the general applicability to a range of dyes through the attachment *via* the carboxylate group. These polymers were processed into non-toxic nanoparticles (between 35 and 73 nm in diameter) through the nanoprecipitation technique with an amphiphilic lipid. The particles were used in *in vivo* imaging *via* tail vein injection into a mouse, and were found to provide clearer images than, for example, indocyanine green. Notably, the blood vessels near the spinal cord were clearly imaged due to the almost total lack of background fluorescence at *ca.* 1380 nm. Notably, the cerebral blood vessels were clearly imaged through the skull, with the fine vascular structure evident, and a malignant brain tumour in a ND2:SmoA1 transgenic mouse diagnosed

(Fig. 4). This study was particularly noteworthy as this type of tumour (medulloblastoma) is the most common type of brain tumour in children. The mice were anatomised to determine the biodistribution of the nanoparticles, and as expected, the particles were found in the liver and spleen, consistent with hepatobiliary clearance.

It was however noted that comparison of the spatial resolution and signal to background ratio to other imaging systems must consider other variables, such as the efficiency of the CCD camera, the concentration of the imaging agent, the software used to process the images and the power/wavelength of the excitation source. This can be seen as a general comment and highlights the issues faced when introducing new imaging probes into well-established scientific protocols and marketplaces. It is essential that new imaging agents fit seamlessly with existing technologies if they are to be widely adopted and their positive attributes exploited.

In conclusion, this new imaging technology, which has evolved from solid state applications such as light emitting devices, has clear advantages over simple molecular dyes. The inherent stability and enhanced brightness associated with the polymers makes these materials ideal for the biological arena when engineered to emit in the biological optical windows. Such nanostructures, unlike simple organic dyes, are also capable of incorporating emerging therapeutics such as gene
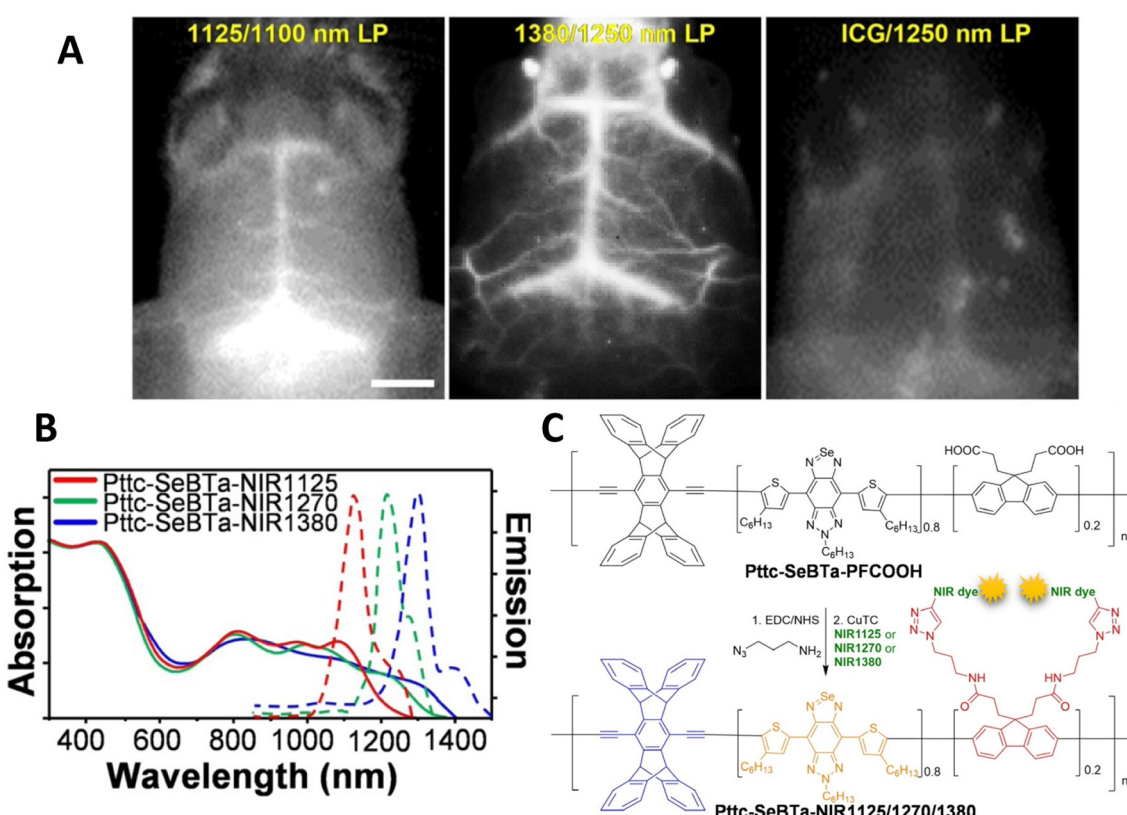

Fig. 4 (A) Near-IR2 image of ND2:SmoaA1 mouse brain vasculature after intravenous injection of near IR emitting conjugated polymer nanoparticles (left hand side, 1100 nm long pass filter. Central panel 1250 nm long pass filter) and ICG dye (right hand side, 1250 nm long pass filter). (B) Optical properties of polymers used in this study. (C) Structures of polymers used in this study.[48] Images used with permission from John Wiley and Sons.

This journal is © The Royal Society of Chemistry 2023

J. Mater. Chem. C, 2023, **11**, 7860–7871 | **7869**

editing and drug delivery and present a wealth of opportunities of which we are only now beginning to realise. Questions do remain though. As the particles are relatively large, can they be cleared? Can they breakdown into species that can be cleared through the reticuloendothelial system, for example. Recent reports have highlighted advances in such areas,[49] but this kind of advances needs to be routine and engineered into the particles. A systematic study into the toxicity of these particles is absent, and if one reads a large selection of reports addressing the use of conjugated polymer nanoparticles of all types (not just infrared emitting) then one reads of the tangential reports that state that no toxic effects were observed. Whilst this is not always clear what studies have been done, the overall anecdotal suggestion is of a nanoparticle imaging system that is devoid of the toxicity issues that have plagued, perhaps unfairly, semiconductor quantum dots. This however requires clarification, which is further complicated by the lack of protocols for nanomaterial toxicity tests. Whilst it is suggested that QDs will not reach the clinic because of their metal constituents, it is hypothesised that it is only a matter of time until conjugated polymer nanoparticles find their way to the clinical and first in human studies. It is perhaps natural to compare CPNs to QDs (as the former have been designed to replace the latter), and the particles reported in this article, and CPNs in general, have yet to undergo the renaissance experienced by their inorganic counterparts. Inorganic QDs are now a sophisticated and mature science with many cutting-edge applications, all due to advances in synthetic chemistry and structure engineering, something CPNs are yet to undergo. The positive aspects of QD science can be extended as goals for CPNs. Primarily, for biological use, CPNs need to be prepared as monodispersed samples of a specific controllable size, that can be tailored with single valence attachment points for targeting molecules for a well-defined disease state. It should be noted that CPN 'synthesis' might more appropriately be considered 'self-assembly' or 'self-organisation', as few bond are either broken or made. Exploitations of these new materials in biology and medicine are also possible, and the review has hinted to uses such as CRISPR and photo-based therapies. It is beyond the view and vision of the authors to suggest future applications with any certainty, and only time will tell.

Conflicts of interest

There are no conflicts to declare.

References

1 H. Kobayashi, M. Ogawa, R. Alford, P. L. Choyke and Y. Urano, *Chem. Rev.*, 2010, **110**, 2620–2640.

2 J. B. Grimm and L. D. Lavis, *Nat. Methods*, 2022, **19**, 149–158.

3 E. Hemmer, A. Benyas, F. Legare and F. Vetrone, *Nanoscale Horiz.*, 2016, **1**, 168–184.

4 J. V. Frangioni, *J. Clin. Oncol.*, 2008, **26**, 4012–4021.

5 G. Hong, A. L. Antaris and H. Dai, *Nat. Biomed. Eng.*, 2017, **1**, 0010.

6 R. C. Benson and H. A. Kues, *Phys. Med. Biol.*, 1978, **23**, 159–163.

7 S. Mindt, I. Karampinis, M. John, M. Neumaier and K. Nowak, *Photochem. Photobio. Sci.*, 2018, **17**, 1189–1196.

8 P. M. Allen, W. Liu, V. P. Chauhan, J. Lee, A. Y. Ting, D. Fukumura, R. K. Jain and M. G. Bawendi, *J. Am. Chem. Soc.*, 2010, **132**, 470–471.

9 G. Hong, S. Diao, J. Chang, A. L. Antaris, C. Chen, B. Zhang, S. Zhao, D. N. Atochin, P. L. Hunag, K. I. Andeasson, C. J. Kuo and H. Dai, *Nat. Photonics*, 2014, **8**, 723–730.

10 Y.-H. Chan and P.-J. Wu, *Part. Part. Syst. Charact.*, 2015, **32**, 11–28.

11 J. Li and K. Pu, *Chem. Soc. Rev.*, 2019, **48**, 38–71.

12 T. Someya, Z. Bao and G. G. Malliaras, *Nature*, 2016, **540**, 379–385.

13 H. Aoki, J. Kakuta, T. Yamaguchi, S. Nitahara and S. Ito, *Polym. J.*, 2011, **43**, 937–940.

14 J. S. Wilson, N. Chawdhury, M. R. A. Al-Mandhary, M. Younis, M. S. Khan, P. R. Raithby, A. Kohler and R. H. Friend, *J. Am. Chem. Soc.*, 2001, **123**, 9412–9417.

15 Y. Jin, F. Ye, M. Zeigler, C. Wu and D. Chiu, *ACS Nano*, 2011, **5**, 1468–1475.

16 L. Xiong, A. Shuhendler and J. Rao, *Nat. Commun.*, 2012, **3**, 1193.

17 C. Ke, C. Fang, J. Yan, P. Tseng, J. Pyle, C. Chen, S. Lin, J. Chen, X. Zhang and Y. Chan, *ACS Nano*, 2017, **11**, 3166–3177.

18 J. Zhang, Y. Huang, D. Wang, A. Pollard, Z. Chen and E. Egap, *J. Mater. Chem. C*, 2017, **5**, 5685–5692.

19 C. Yan, Z. Sun, H. Guo, C. Wu and Y. Chen, *Mater. Chem. Front.*, 2017, **1**, 2638–2642.

20 Y. Lv, P. Liu, H. Ding, Y. Wu, Y. Yan, H. Liu, X. Wang, F. Huang, Y. Zhao and Z. Tian, *ACS Appl. Mater. Interfaces*, 2015, **7**, 20640–20648.

21 K. Li, D. Ding, D. Huo, K.-Y. Pu, N. N. P. Thao, Y. Hu, Z. Li and B. Liu, *Adv. Funct. Mater.*, 2012, **22**, 3107–3115.

22 S. Sindhwani, A. M. Syed, J. Ngai, B. R. Kingston, L. Maiorino, J. Rothschild, P. McMillan, Y. Zhang, N. U. Rajesh, T. Hoang, J. L. Y. Wu, S. Wilhelm, A. Zilman, S. Gadde, A. Sulaiman, B. Ouyang, Z. Lin, L. Wang, M. Egeblad and W. C. W. Chan, *Nat. Mater.*, 2020, **19**, 566–575.

23 J. Liu, G. Feng, D. Ding and B. Liu, *Polym. Chem.*, 2013, **4**, 4326.

24 D. Ding, J. Liu, G. Feng, K. Li, Y. Hu and B. Liu, *Small*, 2013, **9**, 3093–3102.

25 G. Hong, Y. Zou, A. Antaris, S. Diao, D. Wu, K. Cheng, X. Zhang, C. Chen, B. Liu, Y. He, J. Wu, J. Yuan, B. Zhang, Z. Tao, C. Fukunaga and H. Dai, *Nat. Commun.*, 2014, **5**, 4206.

26 A. Ajayaghosh, *Chem. Soc. Rev.*, 2003, **32**, 181–191.

27 M. C. Scharber and N. S. Sariciftci, *Adv. Mater. Technol.*, 2021, **6**, 2000857.

28 J. Yoon, J. Kwag, T. Shin, J. Park, Y. Lee, Y. Lee, J. Park, J. Heo, C. Joo, T. Park, P. Yoo, S. Kim and J. Park, *Adv. Mater.*, 2014, **26**, 4559–4564.

7870 | *J. Mater. Chem. C*, 2023, **11**, 7860–7871

This journal is © The Royal Society of Chemistry 2023

29 J. Pennakalathil, A. Özgün, I. Durmaz, R. Cetin-Atalay and D. Tuncel, *J. Polym. Sci., Part A: Polym. Chem.*, 2015, **53**, 114–122.

30 J. Liu, K. Li and B. Liu, *Adv. Sci.*, 2015, **2**, 1500008.

31 C. Dai, D. Yang, W. Zhang, B. Bao, Y. Cheng and L. Wang, *Polym. Chem.*, 2015, **6**, 3962–3969.

32 T. F. Abelha, C. A. Dreiss, M. A. Green and L. A. Dailey, *J. Mater. Chem. B*, 2020, **8**, 592–606.

33 D. Cui, C. Xie, Y. Lyu, X. Zhen and K. Pu, *J. Mater. Chem. B*, 2017, **5**, 4406–4409.

34 J. Wu, L. You, L. Lan, H. Lee, S. Chaudhry, R. Li, J. Cheng and J. Mei, *Adv. Mater.*, 2017, **29**, 1703403.

35 B. Guo, Z. Sheng, K. Kenry, D. Hu, X. Lin, S. Xu, C. Liu, H. Zheng and B. Liu, *Mater. Horiz.*, 2017, **4**, 1151–1156.

36 Y. Jiang, P. Upputuri, C. Xie, Y. Lyu, L. Zhang, Q. Xiong, M. Pramanik and K. Pu, *Nano Lett.*, 2017, **17**, 4964–4969.

37 D. Gao, P. Zhang, Y. Liu, Z. Sheng, H. Chen and Z. Yuan, *Nanoscale*, 2018, **10**, 19742–19748.

38 B. Guo, J. Chen, N. Chen, E. Middha, S. Xu, Y. Pan, M. Wu, K. Li, C. Liu and B. Liu, *Adv. Mater.*, 2019, **31**, 1808355.

39 C. V. Rohatgi, T. Harada, E. F. Need, M. Krasowska, D. A. Beattie, G. D. Dickenson, T. A. Smith and T. W. Kee, *ACS Appl. Nano Mater.*, 2018, **1**, 4801–4808.

40 L. Li, Z. Yang, S. Zhu, L. He, W. Fan, W. Tang, J. Zou, Z. Shen, M. Zhang, L. Tang, Y. Dai, G. Niu, S. Hu and X. Chen, *Adv. Mater.*, 2019, **31**, 1901187.

41 M. Green, *J. Mater. Chem.*, 2010, **20**, 5797.

42 L. M. Liz-Marzan, M. Giersig and P. Mulvaney, *Langmuir*, 1996, **12**, 4329.

43 F. Lu, C. Zhan, Y. Gong, Y. Tang, C. Xie, Q. Wang, W. Wang, Q. Fan and W. Huang, *Part. Part. Syst. Charact.*, 2020, **37**, 1900483.

44 P. Modicano, P. R. Neumann, M. Schüller, J. Holthof, F. L. Kyrilis, F. Hamdi, P. L. Kastritis, K. Mäder and L. Ann Dailey, *Eur. J. Pharm. Biopharm.*, 2020, **154**, 297–308.

45 D. Chen, Y. Liu, Z. Zhang, Z. Liu, X. Fang, S. He and C. Wu, *Nano Lett.*, 2020, **21**, 798–805.

46 Y. Liu, J. Liu, D. Chen, X. Wang, Z. Zhang, Y. Yang, L. Jiang, W. Qi, Z. Ye, S. He, Q. Liu, L. Xi, Y. Zou and C. Wu, *Angew. Chem., Int. Ed.*, 2020, **59**, 21049–21057.

47 X. Wang, L. C. Groff and J. D. NcNeill, *J. Phys. Chem.*, 2014, **118**, 25731–25739.

48 M. Liu, Z. Zhang, Y. Yang and Y. Chan, *Angew. Chem., Int. Ed.*, 2021, **60**, 983–989.

49 T. Repenko, A. Rix, S. Ludwanoski, D. Go, F. Kiessling, W. Lederle and A. J. C. Kuehne, *Nat. Commun.*, 2017, **8**, 470.

This journal is © The Royal Society of Chemistry 2023

J. Mater. Chem. C, 2023, **11**, 7860–7871 | 7871